New Research Proposal to Jefferson Lab PAC 28

Deeply Virtual Compton Scattering at 6 GeV with polarized target and polarized beam using the CLAS Detector

H. Avakian, S. Boyarinov, V.D. Burkert, L. Elouadrhiri[1, 2] M. Ito, R. Niyazov,
Yu. Sharabian, E. Smith, S. Stepanyan
Jefferson Lab, Newport News, VA 23606, USA

J. Ball, P. Bertin, A. Camsonne, R. De Masi, F. Descamps, M. Garçon, F.-X. Girod,
M. Guidal, H.-S. Jo, M. Mazouz, M. Mac Cormick, B. Michel
C. Muñoz Camacho, S. Niccolai[1], F. Sabatié, E. Voutier
LPC (Clermont) / LPSC (Grenoble) / IPNO (Orsay) / SPhN (Saclay)
CEA/DSM/DAPNIA & CNRS/IN2P3, France

K. Joo[1], N. Markov, M. Ungaro, B. Zaho
University of Connecticut, Storrs, CT 06269, USA

A. Biselli[1]
Fairfield University, Fairfield CT 06824, USA

S. Kuleshov, O. Pogorelko
Institute of Theoretical and Experimental Physics, Moscow, 117259, Russia

H. Aznauryan, N. Dashyan, K. Egiyan
Yerevan Physics Institute, Yerevan, Armenia 375036

V. Koubarovsky, P. Stoler
Rensselaer Polytechnic Institute, Troy, NY 12181, USA

M. Amarian, G. Dodge, H. Juengst, S.E. Kuhn, A. Radyushkin
Old Dominion University, Norfolk, VA 23529, USA

G.V. Fedotov, B.S. Ishkhanov, E.L. Isupov, V.I. Mokeev, N.V. Shvedunov
Skobeltsyn Nuclear Physics Institute at Moscow State University
19899 Vorob'evy gory, Skobeltsyn Nuclear Physics Institute at Moscow State University, Moscow, Russia

[1]Co-spokesperson
[2]Contact person

S. Chen
Florida State University, Tallahassee, FL 32306, USA

L.C. Smith
University of Virginia, Charlottesville, VA 22903, USA

M. Vanderhaeghen
College of William and Mary, Williamsburg, VA 23185, USA

Abstract

We propose to study the target single spin asymmetries (target SSA) in Deep Virtual Compton Scattering (DVCS) using the CEBAF 6 GeV polarized electron beam, a polarized solid state $^{14}NH_3$ target, and the CEBAF Large Acceptance Spectrometer (CLAS) together with the newly built Inner Calorimeter (IC). The main focus of the experiment will be the measurement of the target single spin asymmetry in the reaction $e\vec{p} \rightarrow ep\gamma$. This asymmetry is directly proportional to the imaginary part of the DVCS amplitude, and gives access to a combination of the Generalized Parton Distributions (GPD) $\tilde{H}$, H, and E. The expected asymmetry from the leading-order calculation is in the range of 20 to 40%, depending on the kinematics and on the GPD model used. The Q^2, x_B, and t dependences of the DVCS amplitude will be studied in a wide range of kinematics. In addition, double spin asymmetries (DSA) for $\vec{e}\vec{p} \rightarrow ep\gamma$ will be measured simultaneously, giving access to the real part of the target spin dependent DVCS amplitude. A total of 60 days of new beam time is requested for this experiment.

Contents

1 Introduction **5**

2 Theory and motivation **6**
2.1 Phenomenology of the GPDs 6
2.2 Deeply Virtual Compton Scattering 7

3 Experimental situation **11**
3.1 Recent Experimental Studies from JLab with CLAS 11
3.2 JLab proposals 11
3.3 The HERMES Experiment 11

4 A dedicated DVCS experiment with a longitudinally polarized target and CLAS **13**
4.1 The CLAS configuration 13
4.1.1 CLAS longitudinally polarized target 13
4.1.2 Helmholtz magnet as magnetic shield 15
4.1.3 CLAS Inner Calorimeter 17
4.1.4 Trigger and data acquisition 22
4.2 Event identification, reconstruction, and acceptances 22
4.2.1 Separation of single γ from $\gamma\gamma$ events. 23
4.3 Count rates and statistical errors 25
4.4 Systematic errors 26
4.5 Projected results 27

5 Summary and beam time request **30**

1 Introduction

In recent years, parton distribution functions have been generalized to contain information not only on the longitudinal but also on the transverse distributions of partons in a fast moving hadron. The Generalized Parton Distributions (GPDs) [1, 2, 3] add important piece of information that is missing in one-dimensional parton densities, in particular distribution of partons in the plane transverse to the direction of motion.

The GPDs contain information on the interference between different quark configurations, on the quark transverse position distribution, as well as their angular momentum distribution. GPDs provide a unifying picture for an entire set of fundamental quantities of hadronic structure, such as nucleon form factors, polarized and unpolarized parton distributions, and to various (intrinsic and orbital) spin components of the nucleon.

Deeply Virtual Compton Scattering (DVCS) is one of the key reactions to determine the GPDs experimentally, and it is the simplest process that can be described in terms of GPDs. We propose a measurement of DVCS in Hall B at Jefferson Lab with a 6 GeV longitudinally polarized electron beam, polarized $^{14}NH_3$ target, and the CLAS detector with the newly built Inner Calorimeter (IC), providing a large acceptance for photon detection while running with high luminosity ($1.5{\times}10^{34}$ cm^{-2}s^{-1}).

The first experimental studies of DVCS with a polarized target were performed by the CLAS Collaboration at JLab and the HERMES collaboration at HERA. In particular, a significant target single spin asymmetry (target SSA) was observed from the CLAS data with a 5.7 GeV electron beam and polarized target [4]. The statistical errors, however, are large and do not allow the extraction of kinematical dependences of the target SSA.

The new measurements will map out the DVCS amplitude in the range of Q^2 from 1 to 4 GeV^2, and x_B from 0.15 to 0.55. The main goal will be a study of the x_B and t dependences of the target SSA. These measurements will have a significantly increased sensitivity to the GPD $\tilde{H}$, when compared to beam spin asymmetry measurements [5, 6, 7, 8].

The CLAS detector with the proposed configuration, including the polarized target, the Inner Calorimeter, and a 6 GeV longitudinally polarized electron beam form a unique facility to perform such measurements with a single experimental setup in a wide range of kinematics.

2 Theory and motivation

2.1 Phenomenology of the GPDs

It has been shown [1, 2, 9] that the DVCS amplitude in the forward direction can be factorized in leading-order perturbative QCD (pQCD) into a hard-scattering part that is exactly calculable in pQCD and a non-perturbative nucleon structure part (Figure 1a) described by GPDs.

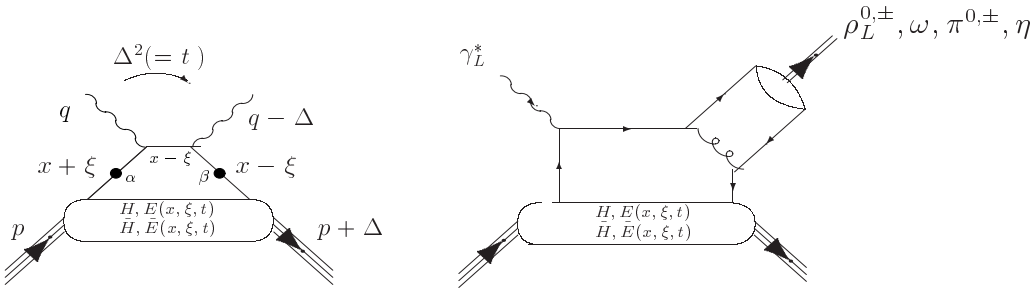

Figure 1: "Handbag" diagrams for (a) DVCS (left) and (b) meson production (right).

There are 4 independent quark-helicity conserving GPDs: $H, \tilde{H}, E$, and $\tilde{E}$ for each quark flavor q. They depend upon three kinematic variables: x, ξ, and t. x characterizes the momentum fraction of the struck quark in the quark loop and, as such, is not directly accessible experimentally except in the measurement of the single-spin asymmetries. ξ is the longitudinal momentum fraction of the transfer Δ, with $\xi = x_B/(2 - x_B)$ in the Bjorken limit. $t = \Delta^2$ is the standard momentum transfer between the virtual and real photons.

H and E are quark-helicity independent (or "unpolarized"), and $\tilde{H}$ and $\tilde{E}$ are quark-helicity dependent (or "polarized") functions.

H and $\tilde{H}$ are generalizations of the parton distributions measured in deep inelastic scattering. In the forward direction (defined by $\Delta = 0$), H^q reduces to the quark longitudinal momentum fraction distribution of the corresponding flavor, and $\tilde{H}^q$ to the quark-helicity distribution, which are measured in deep inelastic scattering:

$$\begin{aligned} H^q(x,0,0) &= q(x) \\ \tilde{H}^q(x,0,0) &= \Delta q(x) \end{aligned} \tag{1}$$

Furthermore, at finite momentum transfer, there are model-independent sum rules that relate the first moments of these GPDs to the standard hadronic form factors.

$$\int_{-1}^{1} H^q(x,\xi,t)dx = F_1^q(t),$$

$$\begin{aligned}
\int_{-1}^{1} E^q(x,\xi,t)dx &= F_2^q(t), \\
\int_{-1}^{1} \tilde{H}^q(x,\xi,t)dx &= G_A^q(t), \\
\int_{-1}^{1} \tilde{E}^q(x,\xi,t)dx &= G_P^q(t), \quad \forall\xi
\end{aligned} \tag{2}$$

Also, Ji [1] has shown that the second moment of these GPDs gives access to the contribution of the sum of the quark spin and the quark orbital angular momentum to the nucleon spin: (Ji's sum rule)

$$\frac{1}{2}\sum_q \int_{-1}^{1} \left(H^q(x,\xi,t=0) + E^q(x,\xi,t=0)\right) x dx \;=\; J_{\text{quarks}} \quad \forall\xi \tag{3}$$

A measurement of this sum would determine the contribution of the quark orbital angular momentum to the nucleon spin. However, we point out that this is not within the goals of the proposed experiment.

The GPDs reflect the structure of the nucleon independently of the reaction that probes the nucleon. They can also be accessed through the hard exclusive electroproduction of mesons, $\pi^{0,\pm}$, $\rho^{0,\pm}$, ω, ϕ,..., (see Figure 1b) for which a QCD factorization proof was given [10]. It also showed that leading-order pQCD predicts that the vector meson channels ($\rho_L^{0,\pm}$, ω_L, ϕ_L) are sensitive only to the unpolarized GPDs (H and E), whereas the pseudoscalar channels ($\pi^{0,\pm}, \eta, ...$) are sensitive only to the polarized GPDs ($\tilde{H}$ and $\tilde{E}$). In contrast to meson electroproduction, DVCS depends on *both* polarized and unpolarized GPDs.

The shape and magnitude of the GPDs also depend on the momentum transfer t. This opens up another dimension in the study of GPDs. The t dependence is particularly sensitive to the transverse distribution of the quarks. For example, a precise knowledge of $H(x,0,t)$ and $\tilde{H}(x,0,t)$ would lead to a determination of the distribution of quark longitudinal momentum fraction and helicity as a function of transverse position (this concept can be extended to $\xi \neq 0$) [11].

2.2 Deeply Virtual Compton Scattering

Deeply Virtual Compton Scattering (DVCS) is the most promising channel for studying GPDs at lower energies and Q^2. The handbag diagram is expected to dominate at lower Q^2 than in the case of deep exclusive meson production.

A complete analysis of DVCS observables, including the asymmetries of interest in this proposal, in terms of Fourier moments with respect to the azimuthal angle, was carried out by Belitsky *et al.* [3], up to the twist-3 approximation. These asymmetries allow one to extract separate components of the angular dependence of the cross section, and project out corresponding distribution functions. The five-fold cross

section for exclusive photon production

$$\frac{d\sigma}{dx_{\rm B}dydtd\phi d\varphi} = \frac{\alpha^3 x_{\rm B} y}{16\,\pi^2\,Q^2\sqrt{1+\epsilon^2}}\left|\frac{\mathcal{T}}{e^3}\right|^2 \tag{4}$$

depends on the Bjorken variable $x_{\rm B}$, the squared momentum transfer $t = (P_2 - P_1)^2$, the lepton energy fraction $y = P_1 \cdot q_1 / P_1 \cdot k$, with $q_1 = k - k'$, and, in general, two azimuthal angles. The amplitude $\mathcal{T}$ is the sum of the DVCS $\mathcal{T}_{\rm DVCS}$ and Bethe-Heitler (BH) $\mathcal{T}_{\rm BH}$ amplitudes.

The azimuthal angular dependence of each of the three terms in

$$\mathcal{T}^2 = |\mathcal{T}_{\rm BH}|^2 + |\mathcal{T}_{\rm DVCS}|^2 + \mathcal{I}\,, \tag{5}$$

with the interference term

$$\mathcal{I} = \mathcal{T}_{\rm DVCS}\mathcal{T}^*_{\rm BH} + \mathcal{T}^*_{\rm DVCS}\mathcal{T}_{\rm BH}\,, \tag{6}$$

is given by [3]:

$$|\mathcal{T}_{\rm BH}|^2 = \frac{e^6}{x_{\rm B}^2 y^2(1+\epsilon^2)^2 t\,\mathcal{P}_1(\phi)\mathcal{P}_2(\phi)}\left\{c_0^{\rm BH} + \sum_{n=1}^{2} c_n^{\rm BH}\,\cos n\phi + s_1^{\rm BH}\,\sin\phi\right\}\,, \tag{7}$$

$$|\mathcal{T}_{\rm DVCS}|^2 = \frac{e^6}{y^2 Q^2}\left\{c_0^{\rm DVCS} + \sum_{n=1}^{2}\left[c_n^{\rm DVCS}\cos n\phi + s_n^{\rm DVCS}\sin n\phi\right]\right\}\,, \tag{8}$$

$$\mathcal{I} = \frac{\pm e^6}{x_{\rm B} y^3 t \mathcal{P}_1(\phi)\mathcal{P}_2(\phi)}\left\{c_0^{\mathcal{I}} + \sum_{n=1}^{3}\left[c_n^{\mathcal{I}}\cos n\phi + s_n^{\mathcal{I}}\sin n\phi\right]\right\}\,, \tag{9}$$

where the $+$ ($-$) sign in the interference stands for the negatively (positively) charged lepton beam. The Fourier coefficients in $|\mathcal{T}_{\rm BH}|^2$ are calculable in QED, while the ones appearing in $\mathcal{I}$ and $|\mathcal{T}_{\rm DVCS}|^2$ depend on so-called Compton form-factors (CFF). At twist-2 level, some of the higher Fourier coefficients are zero, and four CFFs ($\mathcal{H}$, $\widetilde{\mathcal{H}}$, $\mathcal{E}$, $\widetilde{\mathcal{E}}$) describe the process; these CFF are complex quantities, directly related to the four twist-2 GPDs by:

$$\Re{\rm e}\mathcal{H} = \sum_q e_q^2 P \int_{-1}^{+1}\left[\frac{1}{\xi - x} \mp \frac{1}{\xi + x}\right] H^q(x,\xi,t)dx \tag{10}$$

$$\Im{\rm m}\mathcal{H} = \pi \sum_q e_q^2\left[H^q(\xi,\xi,t) \mp H^q(-\xi,\xi,t)\right] \tag{11}$$

and similarly for the three other CFF.

Target single spin asymmetry.

In the case of interest to this experiment, with a longitudinally polarized (LP) target, the single spin asymmetry A_{UL} (sometimes denoted target SSA) is given, still at twist-2 level, by:

$$A_{\rm UL}(\phi) \sim \frac{x_{\rm B}}{y}\,\frac{s^{\mathcal{I}}_{1,\rm LP}}{c^{\rm BH}_{0,\rm unp}+....}\,\sin(\phi)$$
$$\propto \Im{\rm m}\left\{F_1\widetilde{\mathcal{H}}+\frac{x_{\rm B}}{2-x_{\rm B}}(F_1+F_2)(\mathcal{H}+\frac{x_{\rm B}}{2}\mathcal{E})+....\right\}\sin(\phi)\,, \qquad (12)$$

where the dots in the denominator represent known BH terms or smaller interference terms, while the dots in the numerator represent terms proportional to $\widetilde{\mathcal{E}}$, kinematically suppressed by factors of order $x_{\rm B}^2$ or $x_{\rm B}t/4M^2$. Thus, $A_{\rm UL}(\phi)$ is in first approximation a linear function of CFFs with a dominant contribution from $\Im{\rm m}\mathcal{H}$ and $\Im{\rm m}\widetilde{\mathcal{H}}$, that is from the GPDs H and $\tilde{H}$ along the lines $x=\pm\xi$ [3].

Let's recall that for the beam spin asymmetry $A_{\rm LU}$ we have:

$$A_{\rm LU}(\phi)\propto\Im{\rm m}\left\{F_1\mathcal{H}+\frac{x_{\rm B}}{2-x_{\rm B}}(F_1+F_2)(\widetilde{\mathcal{H}}-\frac{\Delta^2}{4M^2}F_2\mathcal{E})+....\right\}\sin(\phi)\,, \qquad (13)$$

At our typical kinematics ($x_B\approx 0.3$) it is easy to check that $A_{UL}\propto\widetilde{\mathcal{H}}+\frac{1}{2}\mathcal{H}$ and therefore, given that $\mathcal{H}\approx 2\widetilde{\mathcal{H}}$ (intuitively, unpolarized distributions are larger than the unpolarized ones), A_{UL} is equally sensitive to $\mathcal{H}$ and $\widetilde{\mathcal{H}}$. Along the same lines, one can show that $A_{\rm LU}$ is mostly sensitive only to $\mathcal{H}$.

Figure 2 shows the relative contributions of the GPDs H and $\tilde{H}$ to the target-spin asymmetry (left panel) and beam-spin asymmetry of DVCS, according to the model in Ref. [16]. The contribution of $\tilde{H}$ to the beam-spin asymmetry is negligible, while for the target spin asymmetry its weight is equal to the one of H.

Double spin asymmetry

With the use of a polarized electron beam, this experiment will also determine the double spin asymmetry $A_{\rm LL}$. Note that a polarized electron beam is needed for the measurement of the target polarization through $\vec{e}\vec{p}$ elastic scattering (see Section 4.1.1). Unlike $A_{\rm UL}$, the Bethe-Heitler process alone can generate a double spin asymmetry $A_{\rm LL}$. At twist-2 level, this observable takes the form:

$$A_{\rm LL}(\phi) \sim \frac{x_{\rm B}}{y}\,\frac{c^{\rm BH}_{0,\rm LP}+c^{\mathcal{I}}_{0,\rm LP}+(c^{\rm BH}_{1,\rm LP}+c^{\mathcal{I}}_{1,\rm LP})\cos(\phi)}{c^{\rm BH}_{0,\rm unp}+....}$$
$$\text{with } c^{\mathcal{I}}_{0,\rm LP} \text{ and } c^{\mathcal{I}}_{1,\rm LP} \propto \Re{\rm e}\left\{F_1\widetilde{\mathcal{H}}+\frac{x_{\rm B}}{2-x_{\rm B}}(F_1+F_2)(\mathcal{H}+\frac{x_{\rm B}}{2}\mathcal{E})+....\right\}\,, \qquad (14)$$

In this expression, the interference terms are expected to be smaller, but not much smaller, than the known BH terms, so that $A_{\rm LL}$ exhibits a measurable sensitivity to $\Re{\rm e}\mathcal{H}$ and $\Re{\rm e}\widetilde{\mathcal{H}}$. We consider the measurement of this observable a by-product of this experiment, and not part of the main objective.

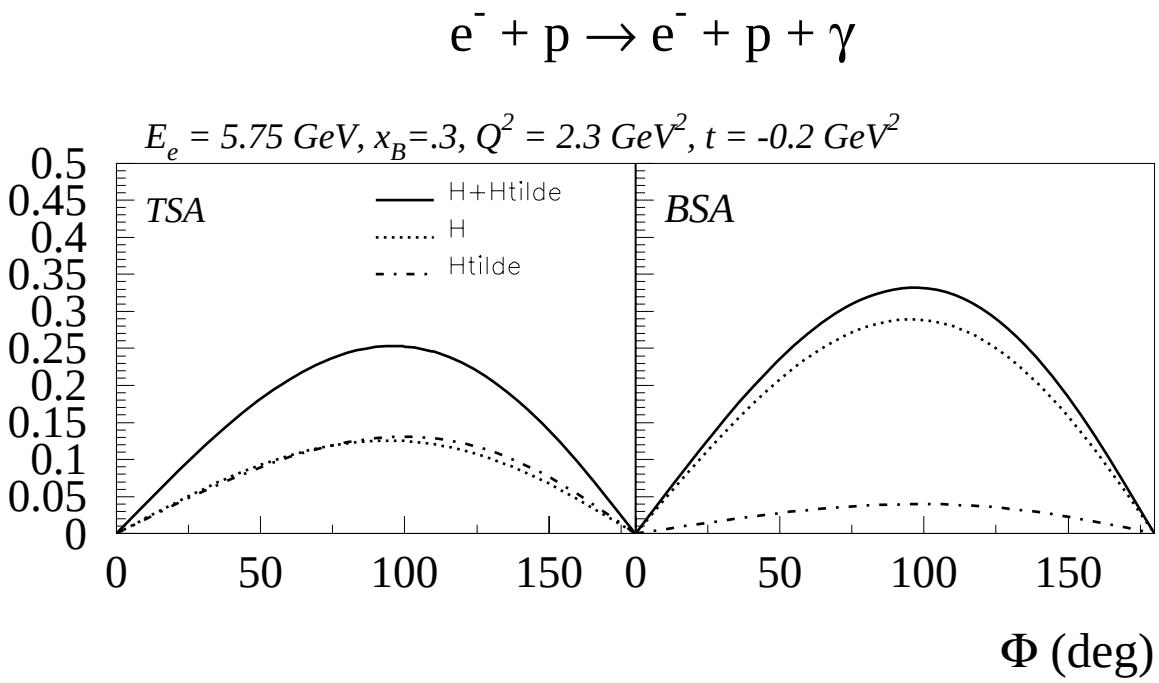

Figure 2: Contributions of the GPDs H and $\tilde{H}$ to the target-spin asymmetry (left panel) and beam-spin asymmetry (right panel) of DVCS.

3 Experimental situation

3.1 Recent Experimental Studies from JLab with CLAS

The DVCS/BH interference with polarized target has recently been measured for the first time both at HERMES [12] and CLAS [4]. The CLAS data were collected as a by-product during the 2000 eg1 polarized target ($^{14}NH_3$) run with 5.725 GeV electrons. At this incident energy, the CLAS acceptance covers a wide range of kinematics in the deep inelastic scattering domain (W $\geq$ 2 GeV and Q^2 $\geq$ 1 GeV^2). The open acceptance of CLAS and the use of a single electron trigger ensures event recording for all possible final states.

For the DVCS analysis, the reaction $e\vec{p} \rightarrow ep\gamma$ was studied, and single photon events were separated using the geometry cut requiring the measured photon to be within a 1° cone relative to the direction calculated of the real photon using the detected scattered electron and the proton. The target single spin asymmetry (target SSA or A_{UL}) is calculated as:

$$A_{UL} = \frac{1}{P_T} \frac{\left(N_\gamma^+ - N_\gamma^-\right)}{\left(N_\gamma^+ + N_\gamma^-\right)} \tag{15}$$

where P_T is the target polarization, and $N_\gamma^{+(-)}$ is the extracted number of $e\vec{p} \rightarrow ep\gamma$ events for positive (negative) target helicity.

The resulting ϕ-dependence is shown in Figure 3 [4] (preliminary results not for circulation). A fit to the function

$$F(\phi) = (A \sin\phi + B \sin 2\phi)/(1 + C\cos\phi) \tag{16}$$

yields $A = 0.237 \pm 0.031$, $B = 0.02 \pm 0.02$, and $C = 0.3 \pm 0.05$. If the handbag diagram dominates, in the Bjorken regime, B should vanish, and only the contribution from transverse photons should remain, described by parameter A.

3.2 JLab proposals

No other proposals at the Jefferson Laboratory are available for the study of the DVCS process with longitudinally polarized target in the valence region.

3.3 The HERMES Experiment

Preliminary target spin asymmetries have been shown by the HERMES Collaboration [12],(see Figure 4).

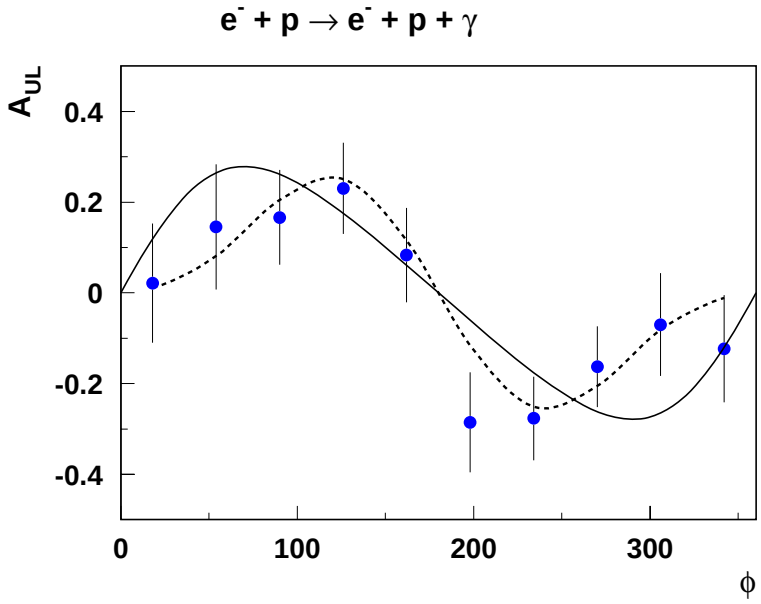

Figure 3: Azimuthal angle (ϕ) dependence of A_{UL} for $e\vec{p} \rightarrow ep\gamma$ at 5.725 GeV in CLAS [4] (preliminary results not for circulation). Data are integrated over the range of Q^2 from 1 to 4 GeV^2, x_B from 0.12 to 0.48 (with the condition $W > 2$ GeV) and $-t$ from 0.1 to 0.6 GeV^2. The dashed curve is the fit to the function $(A \sin\phi + B \sin 2\phi)/(1 + C \cos\phi)$. The solid curve is a GPD-model prediction [16].

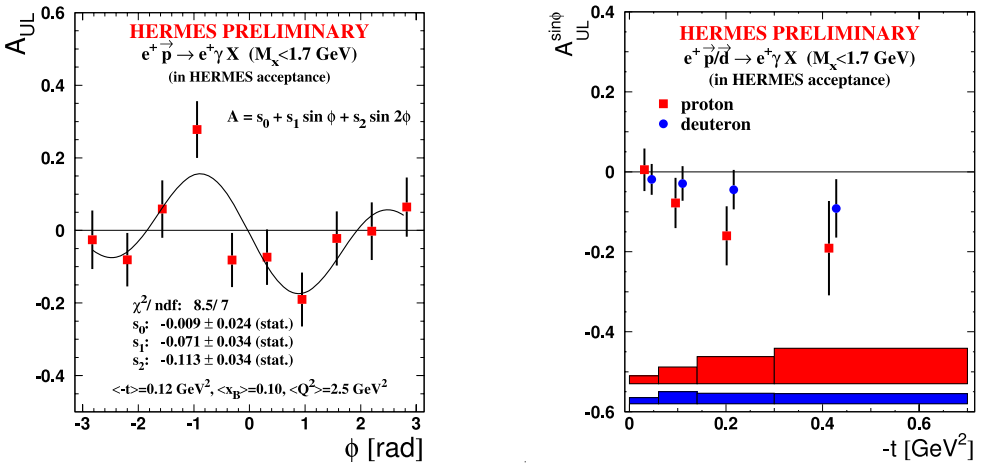

Figure 4: Azimuthal angle ϕ dependence of the $e\vec{p} \rightarrow ep\gamma$ target SSA (A_{UL}) (left) and t dependence of the $ep \rightarrow ep\gamma$ target SSA $\sin\phi$ moment $A_{UL}^{\sin\phi}$ (right) at HERMES.

Since the HERMES Collaboration has currently no plans for running with longitudinally polarized target, no future improvement is expected for this particular observable.

CLAS, together with the CEBAF 6-GeV high-polarization beam is uniquely positioned to perform exploratory measurements of deep exclusive reactions, with a polarized target especially of DVCS.

4 A dedicated DVCS experiment with a longitudinally polarized target and CLAS

The main goal of the proposed experiment is to measure the t and x_B dependences of the target single spin asymmetries (target SSA or A_{UL}) for several fixed Q^2 bins (see Figure 5). We will also obtain the double spin asymmetry (DSA or A_{LL}) for the same Q^2 bins. These quantities are directly sensitive to the model descriptions of the GPDs. This experiment will be the first statistically significant measurements of the kinematic dependences of the target SSA and the DSA in the DVCS process.

A_{UL} will be measured as defined in Eq. 15 and A_{LL} will be measured as:

$$A_{LL} = \frac{1}{P_e P_T} \frac{\left(N_\gamma^{++} + N_\gamma^{--}\right) - \left(N_\gamma^{+-} + N_\gamma^{-+}\right)}{\left(N_\gamma^{++} + N_\gamma^{--}\right) + \left(N_\gamma^{+-} + N_\gamma^{-+}\right)} \tag{17}$$

where P_e is the electron beam polarization, and $N_\gamma^{\pm\pm}$ is the extracted number of $\vec{e}\vec{p} \rightarrow ep\gamma$ events for positive or negative beam (target) helicity.

4.1 The CLAS configuration

4.1.1 CLAS longitudinally polarized target

For this proposed experiment, we will use the same target setup as in the eg1 run and the approved experiment E-03-006 which will measure the low Q^2 GDH sum rule [13]. The setup consists of a target insert which holds four target cells and can be moved by means of a stepping motor to position the different targets in and out of the beam. As target materials we will use polarized solid ammonia ($^{14}NH_3$) as the main target and ^{12}C and an empty cell in order to subtract the nuclear background. We will also use an ^{14}N target, which requires a separate target insert, again for background study purposes. The ammonia target is polarized via the *Dynamic Nuclear Polarization* technique, which requires the target to be cooled down to 1 K, as well as being in a uniform ($\Delta B/B = 10^{-4}$) magnetic field of 5T. The cooling system is a ^4He evaporation refrigerator. The ^4He contribution to the cross section can be subtracted off by combining data from the ^{12}C and *empty* cell targets. The magnetic field is supplied by two Helmholtz-like coils placed axially around the

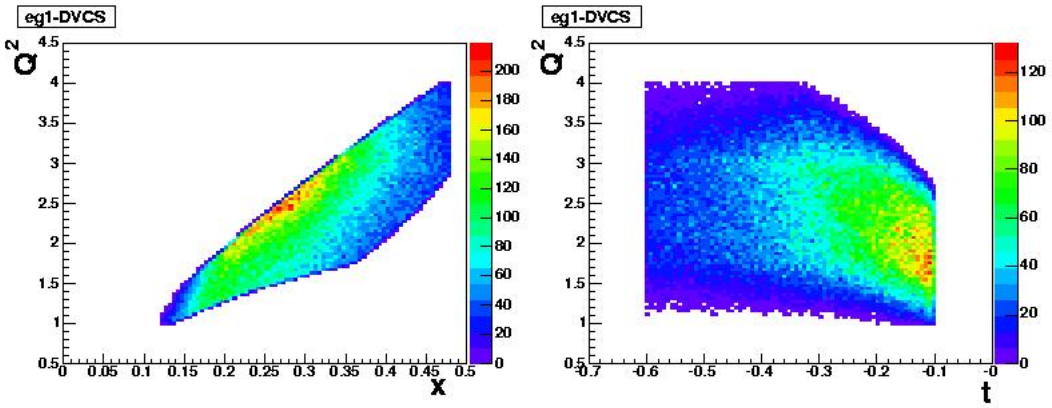

Figure 5: The accessible range of Q^2, x_B and t with CLAS at 6 GeV beam energy, for the proposed eg1-dvcs configuration.

target as in our previously polarized target result [17]. The presence of the coils limits the polar angle, but the available coverage up to 50 deg gives a good acceptance for DVCS events as shown in Fig 6. The Helmholtz field also provides magnetic shielding from background due to Møller electrons as explained in detail in section 4.1.2.

We expect target polarizations of about 70-90% which were already achieved in the eg1b experiment. The target polarization will be continuously monitored with an *NMR* system to get a prompt feedback; however, an accurate estimate of the product of target and beam polarizations, $P_e P_t$, will be done off-line by comparing the well known elastic asymmetry

$$A_{theo} = -\frac{\cos\theta_\gamma\sqrt{1-\epsilon^2} + (\frac{Q^2}{4M^2})^{-\frac{1}{2}}\sqrt{2\epsilon(1-\epsilon)}\sin\theta_\gamma\cos\phi_\gamma\frac{G_E}{G_M}}{\epsilon(\frac{Q^2}{4M^2})^{-1}(\frac{G_E}{G_M})^2 + 1} \tag{18}$$

with the measured asymmetry

$$A_{meas} = \frac{N^+ - N^-}{N^+ + N^-} = \frac{P_e P_t \sigma_{et}}{\sigma_0} \equiv P_e P_t A_{theo}. \tag{19}$$

The ratio $\frac{G_E}{G_M}$ has been measured in many experiments and is known with about 3% accuracy in the Q^2 region of interest [14]. For our Q^2 range, $\frac{G_M}{G_E} \sim \nu_p$ where ν_p is

the magnetic moment of the proton[3]. Figure 7 shows the product $P_e P_t$ for different Q^2 intervals at the beam energy of 5.6 GeV. Since the elastic cross section at high beam energy is very small, additional calibration runs at lower beam energy will also be taken in order to have high statistics data to extract $P_e P_t$.

To avoid radiation damage to the target the beam will be rastered over the target surface in a spiral pattern. The beam position is measured indirectly by recording the simultaneous currents of the raster magnet. These values can be used off-line to correct for effects of the raster on the vertex z-position. Figure 8 shows the z-vertex position before and after correction for the eg1b data set.

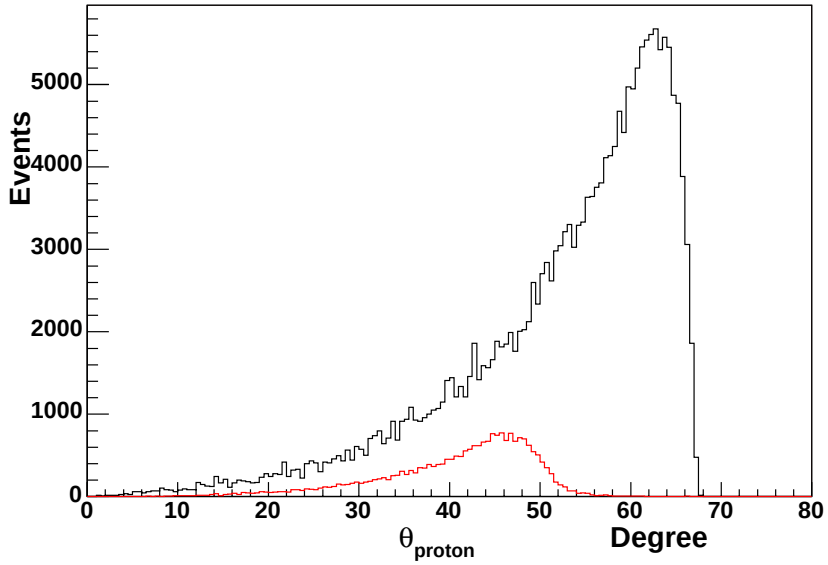

Figure 6: Simulation of DVCS events. The black curve gives the original events, and the red curve gives the accepted ones.

4.1.2 Helmholtz magnet as magnetic shield

The main source of background produced by a high-energy electron beam impinging upon a hydrogen target is due to interactions of the electron beam with the atomic electrons (Møller scattering). This rate is several orders of magnitude larger than the inelastic hadronic production rate. In polarized target running with CLAS, this background is largely eliminated by the target magnetic field shielding the Region I tracking chambers from the charged electromagnetic background. This allowed CLAS to reach the highest luminosities achieved in a large acceptance detector to date.

[3] $\nu_p = \frac{1}{2} g$ where $g = 5.5856912$

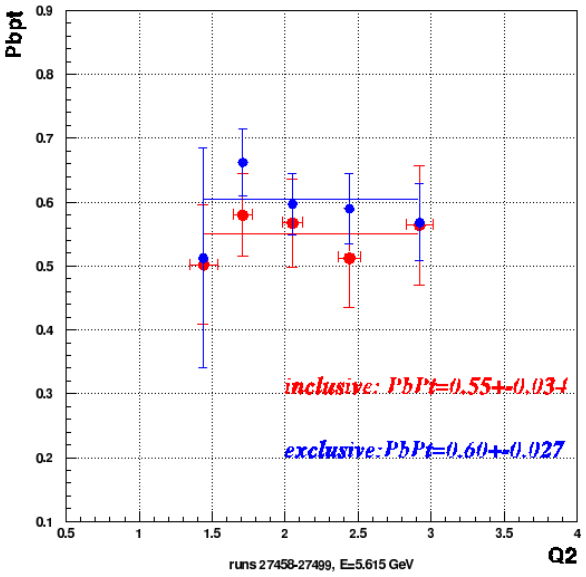

Figure 7: $P_e P_t$ for eg1b data at 5.6 GeV

The eg1 superconducting Helmotz magnet was designed with the goal of generating a homogeneous magnetic field of 5 T at the target location, parallel to the direction of the electron beam. At the same time, it reduced the Møller background in CLAS significantly. Tests during the eg1 experiment showed that the detector could tolerate higher luminosities than during operation with the mini-torus. This behavior had been expected from detailed simulations that were done prior to the installation of the polarized target magnet. Figure 9 shows the luminosity limitations during electron runs using different targets. The polarized target operation at 5.75 GeV (labeled NH_3 in Figure 9) shows approximately a factor of two increased luminosity in terms of a hydrogen-equivalent target material.

For these conditions the simulations show that the Møller electrons are confined to a cone with an opening angle of about 2.5° as seen from a 1 m distance to the production target. Møller electrons, which are the vastly dominating source of electromagnetic background, will pass through the central penetration in the lead-tungstate wall, and will be absorbed in the downstream shielding pipe. The shielding arrangement is the same as the one used during the e1-dvcs experiment [8].

Although the Helmholtz magnet used in eg1 was not optimized as a magnetic shield, but rather to generate a homogeneous magnetic field across the target volume, the shielding absorbs practically all of the Møller electrons as shown in Figure 10 (from our Monte Carlo simulation studies).

The inner calorimeter (IC) designed for the e1-DVCS experiment, will be used with the polarized, target and will significantly increase the kinematic coverage for the direct detection of high-energy photons, the ones from the DVCS process as well as those coming from the decay of high momentum π^0s.

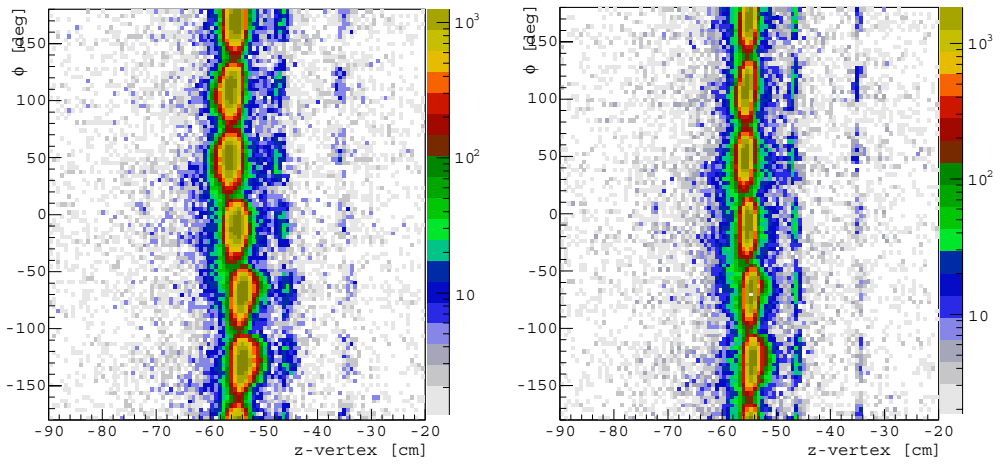

(a) original (b) corrected

Figure 8: Electron z-vertex position for eg1b data before and after the raster corrections

To this end the polarized target will be moved upstream, to allow the installation of the IC within the Region I drift chamber while maintaining sufficient angular resolution to separate single photons from $\pi^o \to \gamma\gamma$ events.

This setup was studied in details during the test run, and the optimal running conditions were identified as shown in Figure 11.

4.1.3 CLAS Inner Calorimeter

A new electromagnetic calorimeter, called inner calorimeter (IC), was built for experiment E-01-113 [8] to measure the DVCS beam single spin asymmetries. Its coverage for photons at small angles (4-16 degrees) ideally complements the standard CLAS electromagnetic calorimeter (EC), and is well suited for the detection of photons from $ep \to ep\gamma$. In addition to the detection of the scattered electrons and the recoil protons in CLAS, the IC (in combination with the EC) makes possible the detection of produced photons in almost the whole phase space. All three particles in the $ep \to ep\gamma$ final state may thus be detected, which is an absolute necessity when using a polarized target.

The IC was built in 2003-2004 by an ITEP/JLab/Orsay/Saclay collaboration, and was operated successfully during the Spring of 2005 for the first part of the e1-DVCS run [8] (a 100-crystal prototype was tested in the fall 2003, in a configuration relevant to this proposal because the polarized target magnet was used to shield the Møller electrons).

A schematic of the IC assembly is presented in Figure 12. The design benefited from R&D for the LHC-CMS experiment, but was innovative in the significantly

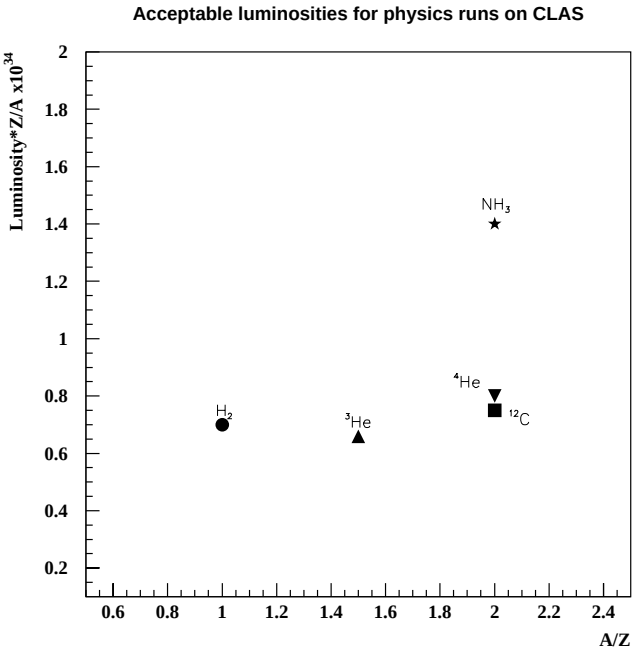

Figure 9: Maximum luminosities used during various electron scattering experiments. The luminosity values are multiplied by Z/A of the scattering target to obtain the hydrogen-equivalent luminosity. The point labeled NH_3 was obtained during operation of a polarized target with longitudinal magnetic field

smaller crystal size, the mechanical assembly, and the preamplifiers. The IC is composed of

- 424 lead tungstate ($PbWO_4$) tapered crystals, 160 mm long (18 radiation lengths), of cross-section 13 mm×13 mm to 16 mm×16 mm,
- light detection through avalanche photo-diodes (APDs),
- low-noise (about 7-8 MeV) fast preamplifiers, allowing a software threshold at 15 MeV/crystal,
- specially designed mechanical structure minimizing the gaps between the crystals,
- a thermal stabilization around 17°C within ± 0.02°C (both the crystal light output and the APD gain vary with temperature, resulting into a signal output variation of about 5%/°C),
- a laser system, used for tests and for monitoring of the relative gains as a function of time,
- standard associated read-out electronics (splitters, Fastbus ADCs - 200 ns gate width - and multihit TDCs).

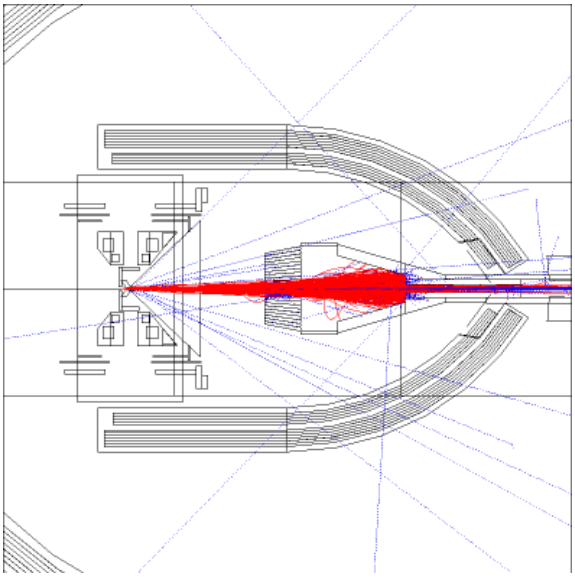

Figure 10: Monte Carlo simulation that shows the Møller electrons in the field generated by the Helmholtz magnet. The target is placed upstream of the center of CLAS ($z = -69$ cm), as well of the calorimeter and its shielding, which are positioned at $z = -10$ cm.

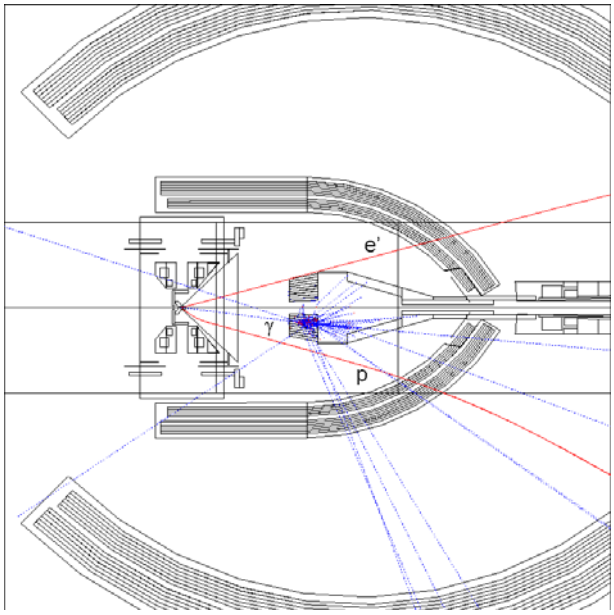

Figure 11: Inner detector layout for the eg1+IC configuration, with single $ep \rightarrow ep\gamma$ event display.

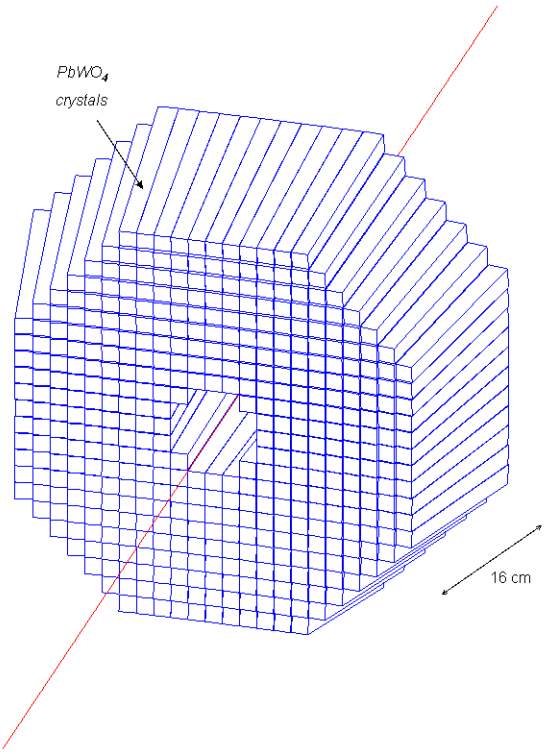

Figure 12: A view of the inner calorimeter.

It will be placed 60 cm downstream of the target center.

Background and radiation damage

The background rates due to Møller electrons are simulated and also measured, with both the polarized target magnet (Helmholtz coils) during the prototype test and with the new "DVCS" solenoid during the e1-dvcs run. Both magnets have similar fringe fields, by design. While the crystals in the inner ring, close to the beam axis, exhibit a pile-up probability of 40-50%, with an exponentially decreasing energy distribution characterized by a mean of 30-40 MeV, this probability falls to about 5-8% in the second ring and becomes negligible at larger angles. Correspondingly, the radiation dose was estimated to be about 50 rad/hour in the inner layer, down to less than 0.1 rad/hour by the fourth ring from the beam axis. Only the inner ring did exhibit some sign of radiation damage (loss of 10% in signal, still under evaluation) during the 70 days of operation of e1-DVCS.

Energy resolution

From GEANT simulations of photon showers [15], an energy resolution of

$$\frac{\sigma_E}{E} = \frac{0.034}{E(\mathrm{GeV})} \oplus \frac{0.038}{\sqrt{E(\mathrm{GeV})}} \oplus 0.022$$

was anticipated. The first term corresponds to the preamplifier noise. The second term is interpreted as fluctuations on the lateral containment of showers, plus a

photostatistics contribution corresponding to 2000 photoelectrons per GeV. The third term is interpreted as fluctuations on energy leakage from the back of the crystals, plus a relative error in gain calibration. Results from e1-dvcs π^0 calibrations (see below) indicate that the achieved resolution is better than anticipated:

$$\sigma_{M_{\pi^0}} \simeq 7.2 \text{ MeV} \Rightarrow \frac{\sigma_E}{E} \simeq 4\% \text{ at } 1 \text{ GeV}$$

Position resolution

The position resolution has also been estimated from simulations [15]:

$$\sigma_x \simeq \frac{2.6 \text{ mm}}{\sqrt{E}} \oplus 0.3 \text{ mm} \quad .$$

This is consistent with the observed π^0 mass resolution from two photon events. At the planned position, 60 cm downstream from the production target, this corresponds to an angular resolution of approximately 3 mr at 2 GeV, which is the minimum energy for the photons of interest. This position resolution, together with a utilization of a cluster algorithm, is sufficient to separate photons from π^0 (1 cluster vs. 2 clusters) up to 5 GeV.

The quality of energy and position reconstruction is illustrated using $ep \rightarrow ep\pi^0$ events from the e1-DVCS data set, comparing π^0 energy and angles calculated on one hand from $ep \rightarrow epX$ kinematics with $X = \pi^0$, and from the measured 2 photons in IC (see Figure 13) on the other hand.

Stability of response

Lead-tungstate crystals are known to be rather sensitive in their light output to temperature changes. The ambient temperature during the e1-DVCS run has been stabilized and monitored. The crystal/APD response has been also carefully checked with light injected into the crystals via quartz fibers, and the response was recorded and used to monitor the gain.

Calibration

The crystal array will be calibrated in-situ using a method developed for the e1-DVCS run: specific runs will be taken with a high-multiplicity the IC trigger. From these $\pi^0 \rightarrow \gamma\gamma$ events will be selected in IC, unrelated to particles detected in CLAS. An iterative procedure allows an adjustment of all individual gains which results in a minimization of the $\gamma\gamma$ invariant mass resolution. The quality of the π^0 mass reconstruction is illustrated in Figure 14, for $ep \rightarrow ep\pi^0$ events, where the two photons are detected either in IC or in EC, or one photon is detected in each calorimeter. IC is seen to have a resolution twice better than EC.

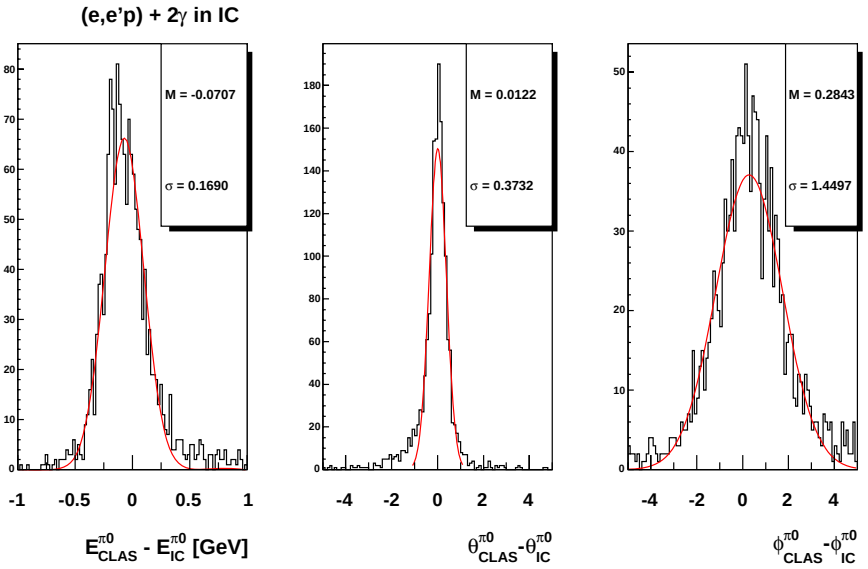

Figure 13: π^0 energy and angle reconstructions in the IC. The abscissa corresponds to the difference between the missing angle/energy calculated from $ep \rightarrow epX$ and the the angle/energy reconstructed from two photons clusters in the IC. The observed resolutions (in GeV and degrees) are a convolution of CLAS and IC resolutions.

4.1.4 Trigger and data acquisition

We are planning to use the standard eg1 production trigger, data acquisition, and online monitoring system of CLAS. The signal amplitude and time information will be read out using standard ADC and TDC boards currently in use in CLAS. The crystal array information will be read out for every event, but not used in the trigger. The standard CLAS level 1 trigger will be used to select scattered electrons. No changes to the trigger hardware are anticipated.

4.2 Event identification, reconstruction, and acceptances

For event identification for $ep \rightarrow ep\gamma$ in CLAS, all three final-state particles will be detected. Electrons are separated from heavier particles using threshold gas Cherenkov counters (CC) and electromagnetic calorimeters, and protons are identified using tracking in the toroidal magnetic field and measurement of time of flight. Charged particle momenta are reconstructed in the CLAS drift chamber system using the standard CLAS reconstruction software. For the proposed experiment, photons from direct production and from π^0 decays (or from η decays) will be reconstructed using the inner calorimeter (IC) and the CLAS forward angle electromagnetic calorime-

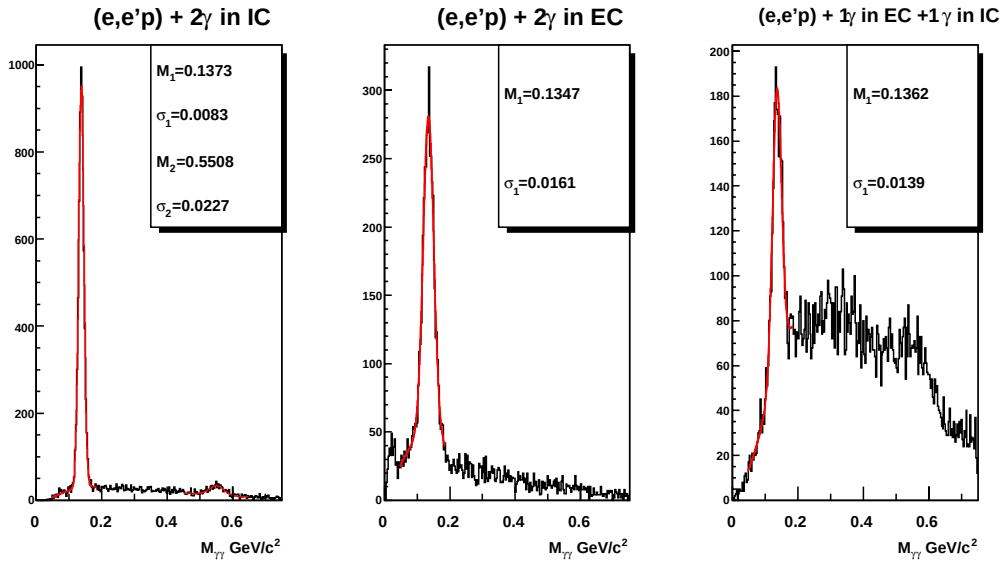

Figure 14: The π^0 resolutions for different configurations. The left plot is for 2 photons in the IC, the middle one for 2 photons in the EC and the right one for mixed configurations.

ter (EC). This will provide large acceptance coverage for both reactions.

One of the main sources of background to the $e\vec{p} \rightarrow ep\gamma$ DVCS/BH processes from the polarized $^{14}NH_3$ target is from single photon events from unpolarized nitrogen. To separate these single photon events from events from polarized hydrogen, we can compare the expected kinematic values (the energy and the polar angle θ) of a "calculated" photon X ($ep \rightarrow epX$) with those of a detected photon γ ($ep \rightarrow ep\gamma$). Due to the Fermi motion of the protons from unpolarized nitrogen, the "calculated" photon X is very different from the detected γ for the events from nitrogen. These background events can be eliminated by selecting events within a 1° cone. Data will be also taken with a solid ^{12}C target for unpolarized-nitrogen background studies aiming to determine the dilution factor.

The missing mass resolution achieved in CLAS is not good enough to separate $ep\gamma$ and $ep\pi^0$ final states event-by-event. Detection of photons in the CLAS EC and the IC will allow separation of single photons from π^0s event-by-event. The e1-6 data analysis and the DVCS MC studies with GSIM indicate that single photons can be separated from π^0s for momenta up to 4 GeV/c by direct reconstruction.

4.2.1 Separation of single γ from $\gamma\gamma$ events.

Accidental coincidences do not play any significant role in electron scattering experiments with CLAS because of the low luminosity and the good time resolution. The

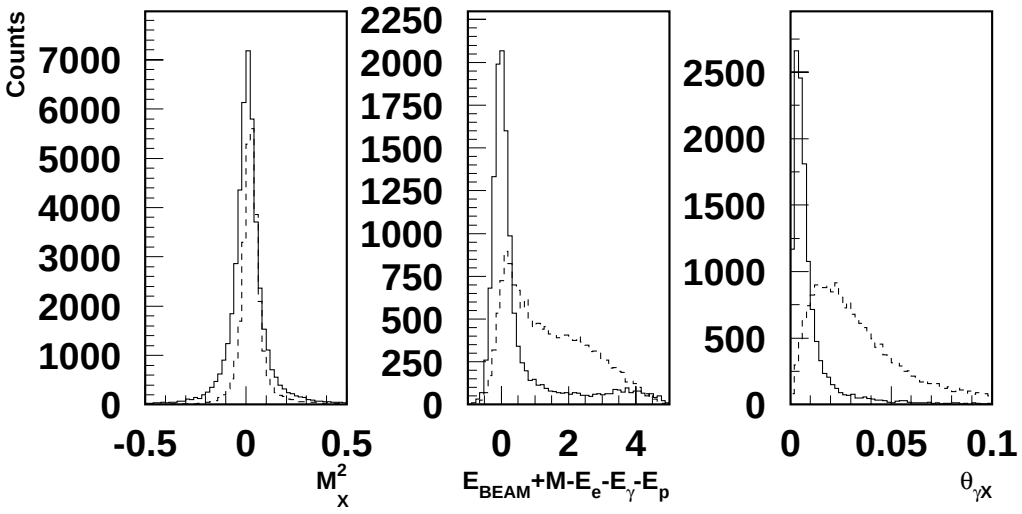

Figure 15: Separation of $ep\gamma$ and $ep\gamma(\gamma)$ events using the missing mass (left), missing energy (middle) and the angle between reconstructed and calculated photons from GSIM.

main sources of background to the $ep\gamma$ final state will be from $ep\pi^0$ and from $ep\gamma\gamma$ events, where only one of the two photons is detected. The former process will be measured directly for the same kinematics as the $ep\gamma$ process, and can be subtracted. The latter reaction corresponds to hadronic production of two photons, which can be measured in the experiment, or inelastic radiative electromagnetic processes. The latter ones are dominated by processes in which the incoming electron radiates off a photon (which escapes detection in the beam pipe) and, for instance, N^* resonances are excited, which subsequently decay into a proton and a photon. The $\gamma\gamma$ final states appear as a continuum in the epX missing mass, so that most of these events will be eliminated by missing mass cuts. The electromagnetic decay is suppressed by typically two orders of magnitude in comparison to a hadronic process. However, the usual radiative corrections are needed to determine the unradiated cross section.

The DVCS MC with polarized target was used to simulate the angular distributions of photons and π^0, and to estimate the possible contamination from π^0 in single photon events.

As can be seen from the first panel of Figure 15, the missing mass cut due to the wide resolution is not particularly useful to separate $ep\gamma$ and $ep\gamma\gamma$ events. Complete kinematical fits, as well as cuts on the missing energy and on the difference between measured and calculated angle, will further improve this separation. Moreover, one can also make use of the required co-planarity for the direct $\gamma^*\gamma p$ events, while $\gamma^*\gamma p$ from $ep\pi^0$ events will generally not be co-planar.

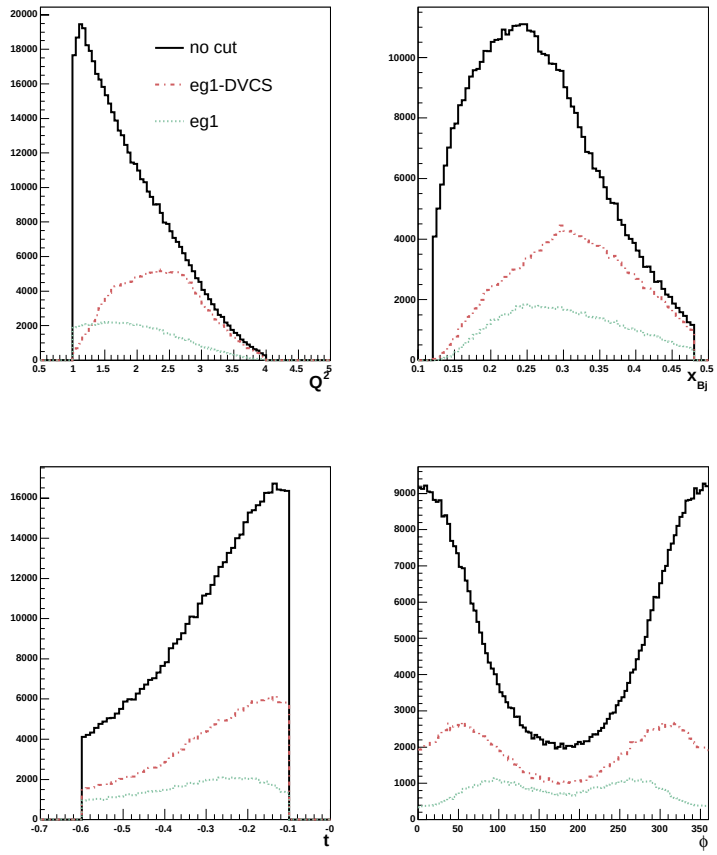

Figure 16: The black, red and green curve represent respectively the generated DVCS events, the accepted events with standard eg1 configuration, and the accepted events with the new setup of the proposed experiment, as function of Q^2, X_{Bj}, t, and Φ. This simulation is adequate to estimate the relative gain when adding IC to the polarized target configuration, but not to infer the absolute acceptance.

4.3 Count rates and statistical errors

The expected number of counts is given by

$$N = \mathcal{L} \times \text{time} \times \sigma \times (\Delta Q^2 \cdot \Delta x_B) \times \Delta t \times \Delta\phi \times (\Delta\varphi_e)_{\text{eff}}/2\pi \qquad (20)$$

With the optimized configuration as described in Sec. 4.1, a luminosity of 1.5×10^{34} $\text{cm}^{-2}\text{s}^{-1}$ is expected.

The resulting number of of DVCS events for the proposed experiment is calculated from the 5 days of the eg1 run scaled to 50 days, and by an additional scale factor due to the increase of photon acceptance in the inner calorimeter. The latter factor is kinematical dependent as shown in figure 16. A beam polarization of 0.8 is assumed for the calculation of $\Delta(TSA)$. All the above factors have been taken into account when calculating the stastical uncertainty.

4.4 Systematic errors

The proposed spin asymmetry measurement is rather insensitive to systematic uncertainties such as acceptances and charge normalization. The main contributions to the uncertainties, summarized in Table 4.4, come from the procedure used to subtract the N and ^{4}He background, from the estimation of target and beam polarization [17], and from possible contamination of the single-photon event sample by misidentified photons from π^0 events. As these events will have a different asymmetry from single photon events they add a systematic error to the asymmetry. The IC will provide the separation of $p\gamma$ and $p(\pi^0 \rightarrow \gamma\gamma)$ events. The π^0 asymmetry will be measured simultaneously and can thus be corrected for, as the size of the π^0 contamination can be measured as well. From the analysis of the 5.7 GeV e1-6 data we conclude that the $ep(\pi^0)$ yield is generally smaller than the $ep(\gamma)$ yield except for some extreme kinematics where it may be comparable or larger. The uncertainty from radiative corrections is normally small ($\approx$ 1%) based on our previous studies for the EG1 experiment.

We conservatively estimate the total systematic error on the asymmetry to be around 7%, sufficiently small for a very significant measurement.

Table 1: Estimated contributions to the systematic uncertainty on the DVCS single spin asymmetry.

Error source	Systematic error (%)
Carbon normalization	4
$P_e P_t$	3
^{4}He background contribution	3
π^0 contamination	3
Radiative corrections	1
Total	< 7

4.5 Projected results

The variation of the asymmetries (TSA and DSA) as a function of the relevant kinematic variables according to different models of GPDs [16], along with the preliminary results from EG1 [4] and a selection of expected data points with the expected statistical accuracy, are shown in the following figures:

- Figure 17 shows the ϕ dependence of the target SSA.
- Figure 18 shows the t dependence of the target single spin asymmetry (target SSA), integrated over all the other variables. In this case it looks possible to distinguish between the different models with the projected error bars.
- Figure 19 illustrates the x_B dependence of the target SSA. Here we will check the general x dependence of the models, which all display the same behavior.
- Finally, Figure 20 shows the t dependence of the double spin asymmetries (DSA or A_{LL}).

x_B and t dependences of the observables.

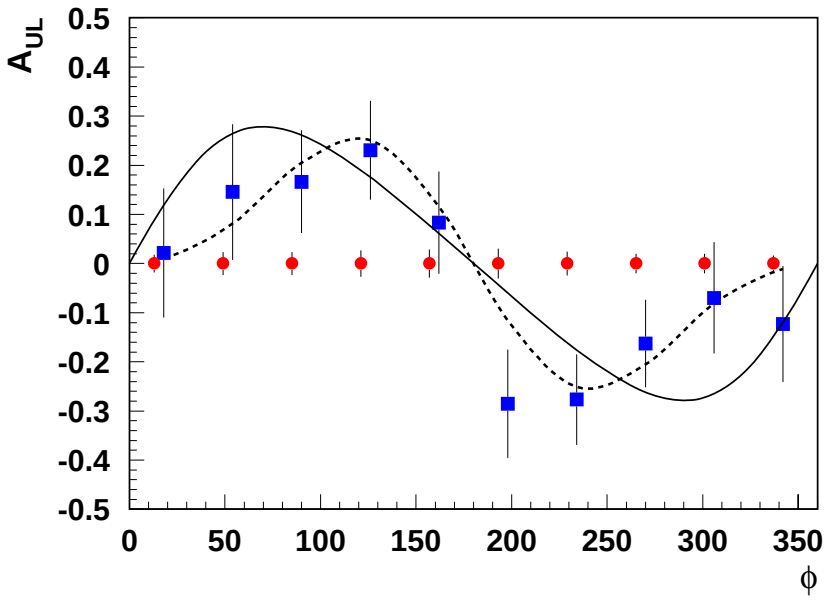

Figure 17: The ϕ dependence of the target SSA. The blue points are the preliminary results of the analysis of the EG1 data [4]. The red points illustrate the statistical accuracy expected for the proposed experiment.

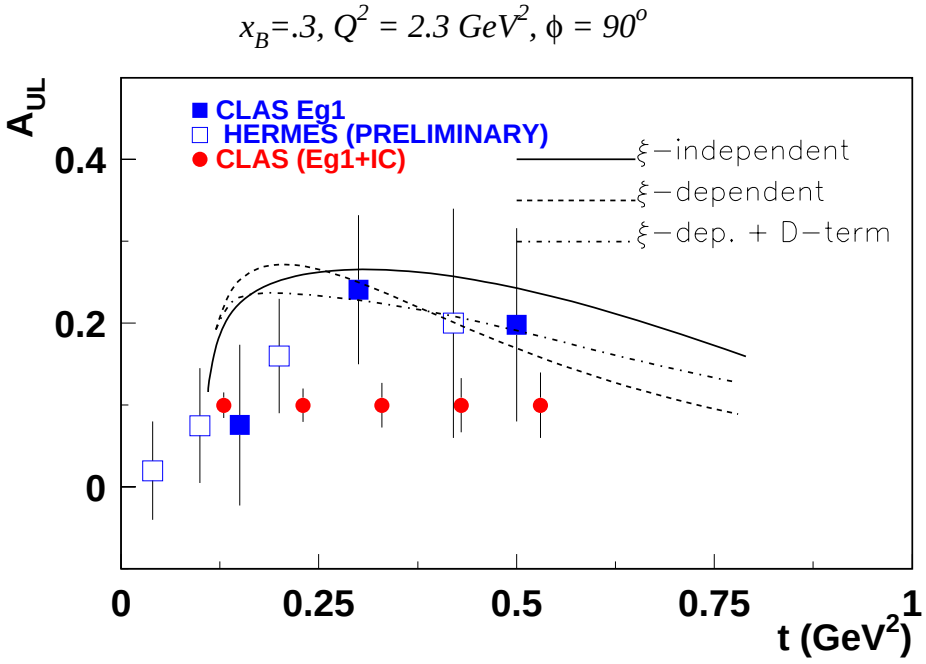

Figure 18: t dependence of the target SSA (A_{UL}) at 6 GeV, for $Q^2 = 2.3$ GeV^2, $x_B = 0.3$ and $\phi = 90°$. The error bars on the red points represent the expected uncertainty on the proposed measurement, the blue full squares are preliminary results from EG1 [4], the blue empty squares are prliminary results from HERMES. The curves are model calculations assuming different parametrizations of GPDs [16].

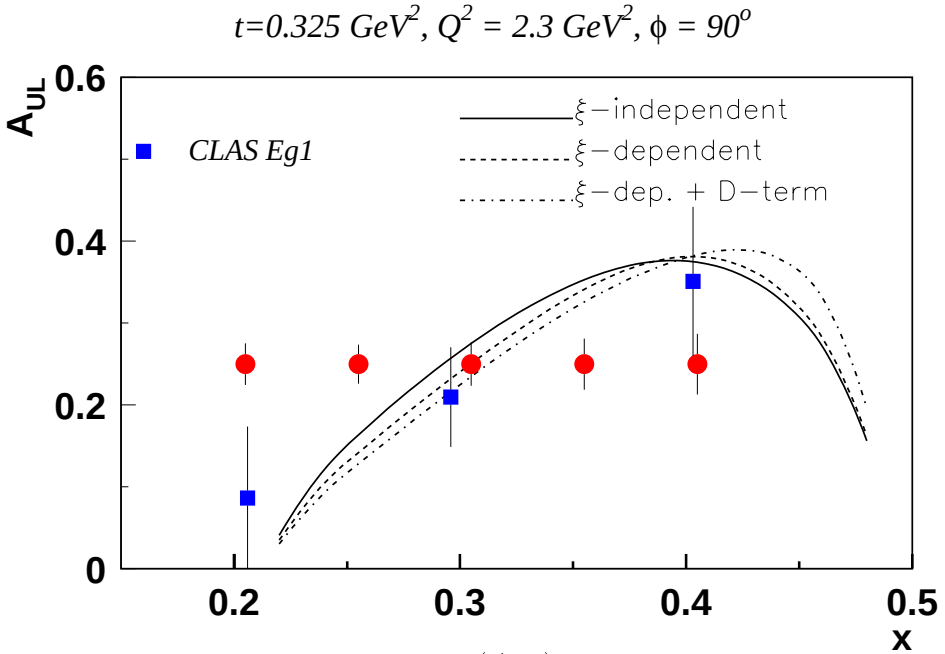

Figure 19: x_B dependence of the target SSA (A_{UL}) at 6 GeV. The red points show the expected accuracy of the proposed measurement, the blue squares are preliminary results from EG1 [4], the theoretical curves are described in the caption of Figure 18.

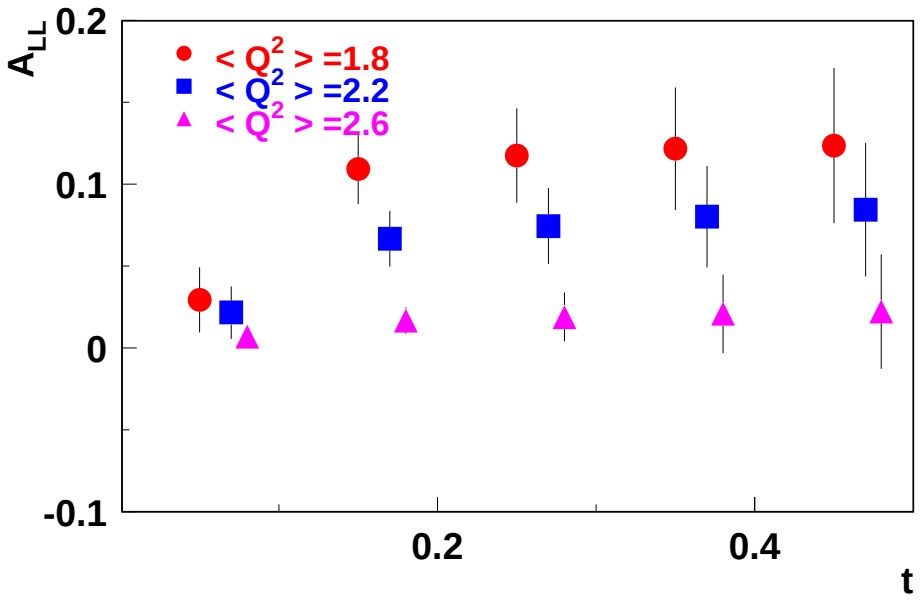

Figure 20: The t dependence of the DSA (A_{LL}) at 6 GeV, for three different Q^2 bins. The points are calculated using the ξ-dependent GPDs of Refs. [16], and the error bars illustrate the expected statistical accuracy.

5 Summary and beam time request

In this experiment we propose a study of the Generalized Parton Distributions (GPD) via measurements of Deeply Virtual Compton Scattering above the resonance region, and for $Q^2 > 1\text{GeV}^2$, using a 6 GeV electron beam and the CLAS detector. The experiment will use CLAS in a modified configuration, with the longitudinally polarized target and the Inner Calorimeter. For this proposal, we request 60 days of beam time with high polarization of electrons at 6 GeV to access the maximum Q^2 range where the formalism of the GPD's is applicable, but where cross sections are particularly low. We expect to improve both the systematic (~ 2) and statistical (~ 4) uncertainties of both HERMES and the eg1 run, thanks to the increased capabilities for the direct detection of high energy photons at small angles (see Fig. 16).

The DVCS process will be determined via interference with the Bethe-Heitler process by measuring the target spin asymmetry. This asymmetry is directly comparable to calculations and predictions in terms of magnitude, Q^2, x_B and t behaviors.

We believe that the measurements that we intend to carry out in this proposal are an indispensable prerequisite for the development of the GPD field and therefore of the understanding of the structure of the nucleon. It should also be clear that this kind of study involves a simultaneous scan of various variables (x_B, Q^2, t) and that a large acceptance detector such as CLAS is most suitable. Analyses of already existing electro-production data from CLAS with polarized target (eg1 data set) and Inner Calorimeter (e1-DVCS data set) as well as the test performed with the polarized-target magnet and the IC prototype have shown that the proposed measurements are feasible.

Table 2: Beam requests and summary of relative merits for the two run periods

Proposal	$\mathcal{L}$ $cm^{-2}sec^{-1}$	relative acceptance (vrs eg1)	beam time scheduled *days*	beam time new *days*	FOM *relative*
eg1+IC run	15×10^{33}	~ 2	5	50	26

The much improved acceptance for photon detection (>2, variable with kinematics), and longer running time (10), compared to the eg1 running, will allow us to extend the kinematic range to higher Q^2 and to map out the x_B and t dependence in smaller bins.

Beam Request

We ask the PAC to award 60 days of beam time for a dedicated high statistics DVCS experiment with the polarized target.

No new equipment is involved and the experiment could be ready in a month.

The proposed DVCS measurement with CLAS will produce precise data on the imaginary part of the DVCS amplitude, that will provide stringent constraints on models for GPDs. Precise data for the DVCS process at 6 GeV will also help maintain the momentum in the theory community. The focus here is on higher-order corrections which likely will be important for a complete understanding of the expected results from the proposed measurement. The studies of DVCS and Deeply Virtual Meson Production are a major driving force for the 12 GeV energy upgrade of CEBAF, and the data at 6 GeV could be crucial for the program.

References

[1] X. Ji, Phys. Rev. Lett. **78**, 610 (1997); Phys. Rev. D **55**, 7114 (1997).

[2] A.V. Radyushkin, Phys. Lett. B **380**, 417 (1996); Phys. Rev. D **56**, 5524 (1997).

[3] A. Belitsky, D. Müller and A. Kirchner, Nucl.Phys. B **629** (2002) 323.

[4] S. Chen *et al.*, in preparation.

[5] A. Airapetian *et al.*, Phys. Rev. Lett. **87**, 182001 (2001).

[6] S. Stepanyan *et al.*, Phys. Rev. Lett. **87**, 182002 (2001).

[7] P. Bertin, C. Hyde-Wright, R. Ransome, F. Sabatié *et al.*, CEBAF experiment 00-110.

[8] V.D. Burkert, L. Elouadrhiri, M. Garçon, S. Stepanyan *et al.*, CEBAF experiment 01-113.

[9] D. Müller *et al.*, Fortschr. Phys. **42** (1994) 2,101.

[10] J.C. Collins, L. Frankfurt and M. Strikman, Phys. Rev. D **56**, 2982 (1997).

[11] M. Burkardt, Int. J. Mod. Phys. **A18**, 173 (2003); M. Diehl, Eur. Phys. J. C **25**, 223 (2002), Erratum-ibid **31** 277 (2003).

[12] M. Kopytin HERMES Coll., talk at the DIS2005 Workshop, Madison (2005).

[13] M. Battaglieri, R.De Vita, A. Deur, M. Ripani *et al.*, CEBAF experiment 03-006.

[14] M.K. Jones *et al.*, Phys. Rev. Lett. **84** (2000) 1398.

[15] F.-X. Girod and M. Garçon, CLAS-Note-2005-001; R. Niyazov and S. Stepanyan, CLAS-Note in preparation.

[16] M. Vanderhaeghen, P.A.M. Guichon and M. Guidal, Phys. Rev. D **60**, 094017 (1999).

[17] A. Biselli *et al.*, Phys. Rev. C 68, 035202 (2003).